Arab J. Nucl. Sci. Appl., Vol. 57, 3, 51-57 (2024)

ISSN 1110-0451

Arab Journal of Nuclear Sciences and Applications

Web site: ajnsa.journals.ekb.eg

(E S N S A)

The Nuclear EOS of PNM and sensitivity of Neutron Star Properties to modern NN Potentials

A. E. Elmeshneb

[1] *Department of Physics, College of Science, Yanbu Branch, Taibah University, KSA.*
[2] *Department of Physics, Faculty of Science, Sohag University, Sohag 82524, Egypt.*

ARTICLE INFO

Article history:
Received: 19th May 2024
Accepted: 27th June 2024
Available online: 6th July 2024

Keywords:
Neutron stars;
Brueckner-Hartree-Fock;
Three-body forces;
Tolman-Oppenheimer-Volkov;
Nuclear interactions;
CD-Bonn NN potentials.

ABSTRACT

In this paper, we utilize the Brueckner-Hartree-Fock (BHF) method to compute the static properties of neutron stars (NS) at zero temperature. We specifically apply a microscopic equation of state for pure neutron matter (PNM). Three-body forces have also been included at different densities. To accurately replicate the nuclear matter saturation point, we have incorporated recent and realistic two-body nuclear interactions. Specifically, we have used the Argonne V18 and CD-Bonn NN potentials, integrated via the Urbana model, to account for the three-body force. We have calculated the properties of neutron stars by numerically solving the Tolman-Oppenheimer-Volkov structure equations. Our results indicate a maximum mass configuration of M = 1.7 ± 0.05 $M_\odot$ (M = 2.12 ± 0.04 $M_\odot$) when using CD-Bonn (Argonne 18) interaction, respectively. These values are consistent with the observed range of neutron star masses. Furthermore, we have discussed the sensitivity of using modern NN potentials and compared our results with other theoretical predictions and observed data.

I. INTRODUCTION

Understanding the Equation of State (EOS) for nuclear matter has profound implications for astrophysics. This fundamental equation is vital in interpreting laboratory-scale nuclear properties and the sophisticated workings of celestial phenomena. The EOS provides critical insights into the macroscopic behavior of nuclei, guiding our understanding of their stability and dynamics. Moreover, within astrophysics, the EOS is paramount in unravelling phenomena such as supernovae and the properties of neutron stars. Neutron stars, known for their extreme densities, serve as cosmic laboratories for testing the limits of our understanding of physics under extreme conditions. Through careful exploration of the EOS, researchers gain invaluable insights into the underlying physics governing these cosmic entities, facilitating a deeper comprehension of the universe's most crucial phenomena. Thus, the EOS for nuclear matter stands as a cornerstone in nuclear physics and astrophysical research, offering a pathway to unlock the mysteries of the cosmos.

The dependence of the nuclear equation of state on density plays a crucial role in the stability of neutron stars against gravitational collapse. At nuclear matter density, employing only realistic two-body forces in the nuclear EOS does not yield the correct saturation point as derived from phenomenological data on various nuclei [1]. Three-body forces (TBF) significantly impact the effective nucleon-nucleon interaction within the medium across several theoretical frameworks, including Brueckner-Hartree-Fock (BHF) [2], Dirac-BHF [3, 4], variational methods [5, 6], and Monte Carlo techniques [7, 8]. Phenomenological TBFs have been utilized to accurately determine the saturation point of nuclear matter and to adjust the overall equation of state for both symmetric and asymmetric nuclear matter, as well as pure neutron matter (PNM). It is essential to study nuclear matter, obtain accurate equations of state, and predict structures based on dense matter properties to understand neutron stars. Therefore, in this study, we adopt a more traditional approach by positing that the core of the neutron star composed solely an idealized infinite, homogeneous system of neutrons, treated as a gas of interacting fermions at T = 0 K. This system's properties are determined by the neutron-neutron interaction and are defined as pure neutron matter (PNM) [10, 11]. It is important to accurately study nuclear matter and obtain an

Corresponding author: AlaaEldeen.elmeshneb@gmail.com
DOI: 10.21608/AJNSA.2024.290999.1820
©Scientific Information, Documentation and Publishing Office (SIDPO)-EAEA

accurate EOS to understand neutron stars and predict the structure of dense matter [12, 13].

The nuclear EOS is calculated for the pure neutron matter within the Bethe-Brueckner-Goldstone (BBG) expansion, which includes the effects of three-body forces. Details of this calculation are provided in Sec. II, the EOS is calculated using modern NN interactions like Argonne V18 and CD-Bonn potentials. This work is an extension of our calculations in [11], but with a very high densities, that it is suitable for studying the composition of neutron stars. The properties of the neutron stars based on a microscopic EOS and the mass-radius relation will be explained in Sec. III with the comparison to other NN potentials.

II. EQUATION OF STATE

The BBG theory, developed by Brueckner and Bethe with Goldstone's contributions, provides a connected cluster expansion for the energy per nucleon in nuclear matter [14]. Within this framework, specific categories of interconnected diagrams are meticulously aggregated, culminating in a closed-form expression extended to infinite orders. This results in the determination of the reaction matrix G, which plays a pivotal role in the theory's formulation.

$$G(n;\omega) = v + v\sum_{K_aK_b} \frac{|K_aK_b> Q <K_aK_b|}{\omega - e(K_a) - e(K_b) + i\eta} G(n;\omega) \qquad \textbf{(1)}$$

Within the framework of Brueckner-Bethe-Goldstone (BBG) theory, the expression governing the reaction matrix G comprises multiple components. One constituent encompasses the original nucleon-nucleon interaction denoted as v, while density of nucleons represented by n, and the initial energy parameter ω. Another integral term involves the Pauli operator | k_ak_b > Q < k_ak_b |. The single-particle energy e(k) within this equation combines kinetic and potential energy components, denoted as U(K).

$$\text{U(K)}.\ \boldsymbol{e}(\kappa) = \boldsymbol{e}(\boldsymbol{k};\boldsymbol{n}) = \frac{\hbar^2}{\boldsymbol{2m}}\kappa^2 + \boldsymbol{U}(\kappa;\boldsymbol{n}) \qquad \textbf{(2)}$$

The single particle potential (s.p.) U(K) plays a crucial role within the framework of the Brueckner Hartree Fock (BHF) approximation. To ensure the continuity at k = kf, U(K) can be formulated as follows:

$$\boldsymbol{U_{BHF}}(\kappa;n) = \sum_{\kappa\prime\leq kf} \langle\kappa\kappa'|\, \boldsymbol{G}(\boldsymbol{n};\boldsymbol{e}(\kappa) + e(\kappa'))|\kappa\kappa'\rangle_a \qquad \textbf{(3)}$$

The subscript "a" denotes the process of antisymmetrizing the matrix element within the Brueckner Hartree Fock (BHF) approximation, it is imperative to solve equations (1) through (3) in a self-consistent manner. Once the auxiliary self-consistent potential is introduced, the calculation of the binding energy per nucleon can be carried out utilizing the subsequent equation:

$$\frac{\boldsymbol{E}}{\boldsymbol{A}} = \frac{\boldsymbol{3}}{\boldsymbol{5}}\frac{\hbar^2}{\boldsymbol{2m}}k_f^2 + D_{BHF} \qquad \textbf{(4)}$$

$$D_{BHF}(n) = \tfrac{1}{2}\tfrac{1}{A}\ \sum_{k.\kappa\prime\leq kf} \langle\kappa\kappa'|\, \boldsymbol{G}(\boldsymbol{n};\boldsymbol{e}(\kappa) + \boldsymbol{e}(\kappa'))|\kappa\kappa'\rangle_{\boldsymbol{a}} \qquad \textbf{(5)}$$

Numerous studies have investigated the inclusion of three-hole line contributions within the Bethe-Brueckner-Goldstone (BBG) expansion [15, 16]. These studies have indicated that such contributions are largely insignificant, with the BBG expansion achieving convergence. However, nonrelativistic calculations relying on two-body forces (2BF) have encountered difficulties in accurately reproducing the saturation point of symmetric nuclear matter [17]. Despite the fact that the binding energy per particle closely matches the empirical value of approximately -16 MeV at the minimum of the saturation curve, the density corresponding to it exceeds the empirical value by approximately 30 to 40 times. To reconcile this inconsistency, the incorporation of three-body forces (TBF) becomes necessary [15, 18]. Various types of TBFs have been employed in nuclear matter calculations, including semi-phenomenological TBFs such as the Urbana TBF [5] and microscopic TBFs [19, 20] rooted in meson exchange theory for NN interactions. Phenomenological TBFs have been utilized to replicate the saturation point of nuclear matter and rectify the entire equation of state for both symmetric and asymmetric nuclear matter [9]. However, achieving accurate reproduction of experimental binding energies of light nuclei and correcting saturation points using a single straightforward set of TBF appears to be exceedingly challenging [21].

In recent years, significant advancements have been achieved in theoretical frameworks. One notable approach, the phenomenological TBF method, utilizes meson exchange principles to analyze NN interactions. This approach has demonstrated effectiveness in replicating key characteristics of nuclear matter, including the saturation point and properties such as binding energies and radii of light nuclei. It operates through an attractive component (V^2_{ijk}) resulting from a two-pion exchange involving the excitation of an intermediate Δ-resonance alongside a repulsive central term (V^R_{ijk}) based on phenomenological considerations.

$$\boldsymbol{V_{ijk} = V_{ijk}^{2\pi} + V_{ijk}^{R}} \quad \textbf{(6)}$$

The component of the TBF stemming from two-pion exchange can be represented through a cyclic iteration across nucleon indicators i, j, and k, involving combinations of anticommutator and commutator terms. Specifically, the formulation for the two-pion exchange contribution to the TBF is given as follows:

$$\boldsymbol{V_{ijk}^{2\pi}} = A \sum cyc \left(\{X_{ij}, X_{jk}\}\{\tau_i.\tau_j,\ \tau_j.\tau_k\}\right.$$
$$\left. + \frac{1}{4}\,[X_{ij}, X_{jk}][\tau_i.\tau_j,\ \tau_j.\tau_k]\right), \quad \textbf{(7)}$$

Where

$$X_{ij} = Y(r_{ij})\sigma_i \cdot \sigma_j + T(r_{ij})\, S_{ij} \quad \textbf{(8)}$$

The operator Xij denotes the one-pion exchange, while σ and τ stand for the Pauli spin and isospin operators, respectively. The tensor operator is represented as $S_{ij} = 3[\,(\sigma_i \cdot r_{ij})(\sigma_j \cdot r_{ij}) - \sigma_i\sigma_j\,]$. Furthermore, Y(r) and T(r) signify the Yukawa and tensor functions, respectively, which are linked to the one-pion exchange similar to the two-body potential. And the repulsive term is given by

$$\boldsymbol{V_{ijk}^{R}} = U \sum cyc\ \ T^2(r_{ij})T^2(r_{ji}) \quad \textbf{(9)}$$

It is mentioned that in the Brueckner Hartree Fock approach, the parameters A and U can be adjusted to match observed nuclear properties and correct the saturation point. Here, we utilize the parameters A (less than 0) and U (greater than 0) alongside NN potentials. A prior study [11] employed a phenomenological three-body force (TBF) in the scenario of pure neutron matter, employing the Argonne V18 and CD-Bonn nucleon-nucleon potentials with and without TBF. Results indicated a significant reduction in discrepancies between equations of state (EOS) obtained from the two potentials, not just in the vicinity of saturation, but also throughout an extensive range of densities. In our current work, we adopt the same TBF model for pure neutron matter, spanning a broad range of densities typical of neutron star interiors. The resulting EOS's obtained using the Argonne V18 and CD-Bonn NN potentials for pure neutron matter are depicted in Figure 1.

The CD-Bonn interaction's non-local nature can lead to a softer EOS at high densities compared to the Argonne V18 interaction. This divergence arises from the CD-Bonn interaction's non-locality introduces more short-range components than the Argonne V18 interaction, which leads to more binding at high densities. Conversely, the Argonne V18 interaction has a stronger tensor force that leads to more repulsion at high densities, making the EOS stiffer [22].

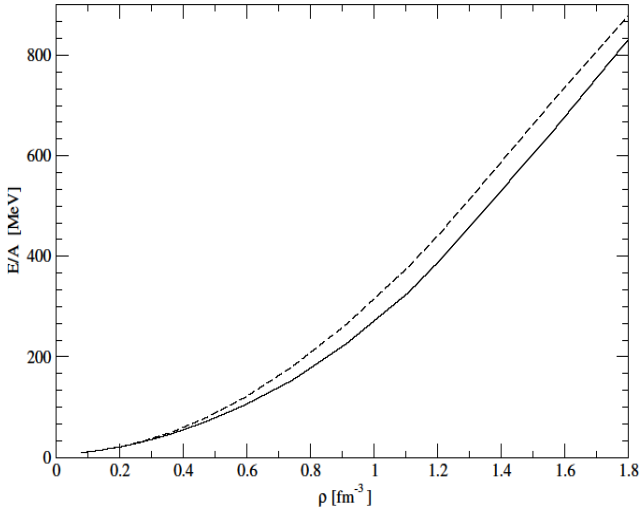

Fig. (1): illustrates the energy per particle (E/A) plotted against density for pure neutron matter. The outcomes are derived by incorporating TBF alongside the realistic CD-Bonn non-local potential (indicated by the solid line) and Argonne V18 local potential (represented by the dashed line), respectively.

The expression for the energy per nucleon of asymmetric nuclear matter (ANM) is stated as follows:

$$\boldsymbol{\frac{E}{A}(n\,.\beta) = \frac{E}{A}(n.\beta = 0) + E_{sym}\beta^2} \quad \textbf{(10)}$$

We introduced the asymmetry parameter

$$\boldsymbol{\beta = \frac{n_n - n_p}{n}} \quad \textbf{(11)}$$

In the context where n_p and n_n are not equal, with n_p representing the proton number density and n_n representing the neutron number density, and where β = 1 denotes neutron matter while β = 0 denotes symmetric matter. The nuclear symmetry energy, $E_{sym}(n)$, characterizes the energy cost associated with changing the proton-neutron asymmetry of nuclear matter.

$$\boldsymbol{E_{sym}(n) \equiv \frac{1}{2}\frac{\partial^2 E/A}{\partial \beta^2}\Big|_{\beta=0}} \quad \textbf{(12)}$$

This energy can be characterized as the disparity between the energy per nucleon of pure neutron matter

and that of symmetric nuclear matter at equivalent densities. Mathematically, it can be formulated as:

$$\boldsymbol{E_{sym}}(n) = \frac{E}{A}(n.\boldsymbol{\beta} = 1) - \frac{E}{A}(n.\boldsymbol{\beta} = 0) \quad \textbf{(13)}$$

The stellar matter's pressure (P) can be determined by relating it to the energy per nucleon. This can be expressed through the following equation, providing insight into the internal dynamics of celestial bodies.

$$\boldsymbol{P} = \rho^2 \frac{\boldsymbol{d(E/A)}}{\boldsymbol{d\rho}} \quad \textbf{(14)}$$

In Figure 2, the pressure of PNM is depicted for the two nuclear interaction models, with density (ρ) as the independent variable. Our findings concerning P(ρ) using the CD-Bonn model align closely with those of [10], using the same potential.

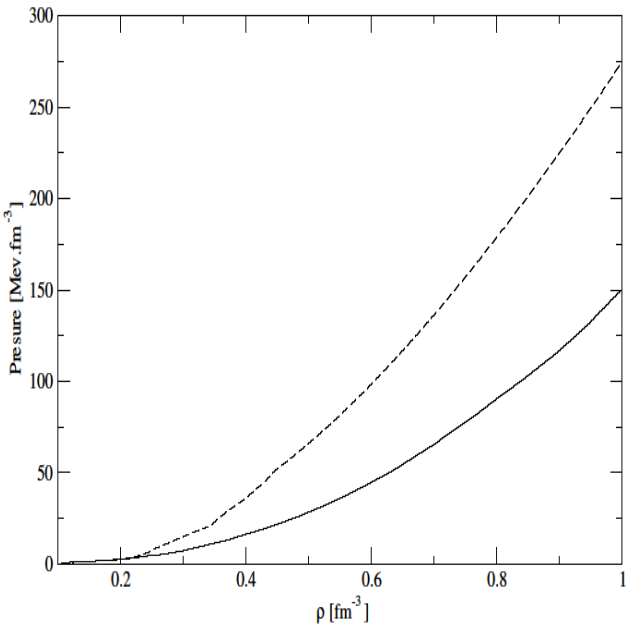

Fig. (2): illustrates the Pressure plotted against density for pure neutron matter. Our results are obtained with inclusion of TBF alongside the realistic CD-Bonn non-local potential (indicated by the solid line) and Argonne V18 local potential (represented by the dashed line), respectively.

III. THE PROPERTIES OF NEUTRON STARS

Following a supernova explosion [23], the core collapse of a massive star gives birth to a neutron star. This phenomenon occurs exclusively in stars with adequate mass, typically estimated to be between 8 and 25 times that of the sun, as they near the conclusion of their lifecycle. The compact nature of neutron stars enables them to resist gravitational collapse through mechanisms rooted in nuclear physics. This unique characteristic transforms neutron stars into ideal environments for scrutinizing the behavior of nuclear matter [23].

Moreover, the structural attributes of a non-rotating neutron star are accessible through a computational approach. Researchers achieve this by numerically integrating the hydrostatic equilibrium equation within the framework of general relativity, employing the Tolman-Oppenheimer-Volkoff equations [24, 25]. The structural details allows for a deeper understanding of the internal dynamics and stability mechanisms governing neutron stars, contributing valuable insights to astrophysical research.

$$\frac{dP}{dr} = -G\frac{m(r)\varepsilon(r)}{c^2r^2}\left(1+\frac{P(r)}{\varepsilon(r)}\right)\left(1+\frac{4\pi r^3P^3(r)}{c^2m(r)}\right)\left(1-\frac{2Gm(r)}{c^2r}\right)^{-1} \quad \textbf{(15)}$$

And

$$\frac{dm(r)}{dr} = \frac{4\pi}{c^2}r^2\varepsilon(r). \quad \textbf{(16)}$$

Determining a neutron star's properties such as mass and radius involves a process where central density is a variable. It assumes a spherically symmetrical mass distribution in hydrostatic equilibrium, disregarding rotational effects and magnetic fields. This procedure entails integrating Equations (15) and (16) until the surface pressure equals that corresponding to the density of iron. Essential in this computation are the gravitational constant, G, and the gravitational mass, m(r). The outcome of this integration provides values for the neutron star's radius and gravitational mass. The pertinent equations (15) and (16) can be located within the Tolman-Oppenheimer-Volkoff framework [24, 25].

$$M_G \equiv m(R) = \frac{4\pi}{c^2}\int_0^R dr\, r^2\varepsilon(r) \quad \textbf{(17)}$$

The Eqs. (15) and (16) describing the neutron star structure were integrated using the microscopic EOS for pure neutron matter, as illustrated in the preceding section, to simulate the core of the neutron star.

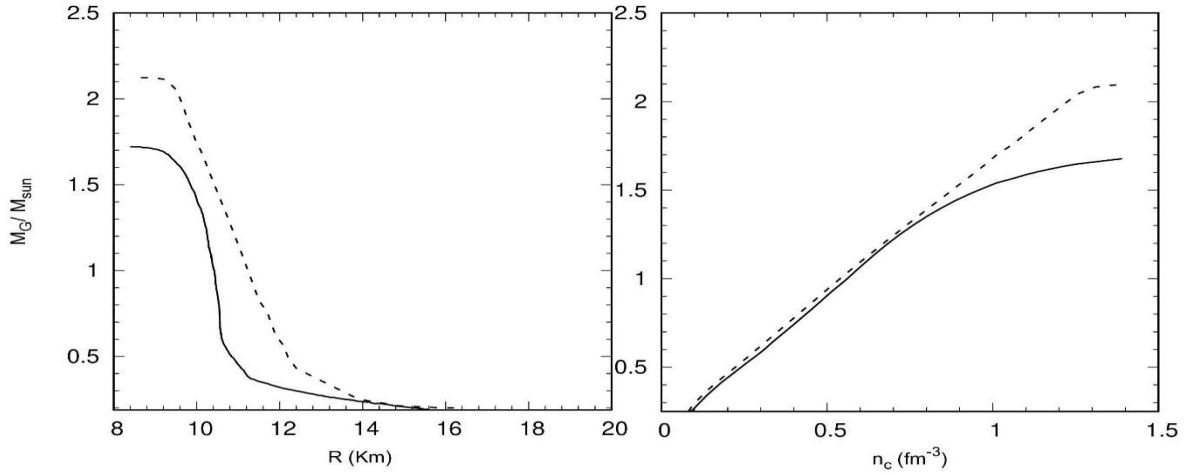

Fig. (3): illustrates the gravitational mass, M_G, in solar mass units ($M_\odot$), plotted against both the radius, R, and the central density, n_c. These results stem from employing EOS for Brueckner calculations, incorporating TBF for the pure neutron matter. Two realistic potentials, Argonne V18 (local) and CD-Bonn (nonlocal), are utilized in these EOS.

The results are depicted in Figure 3, where the gravitational mass, M_G, expressed in solar mass units ($M_\odot = 1.99 \times 10^{33}$ g), is plotted against both the radius, R (left panel), and the central density, n_c (right panel). The solid line represents the CD-Bonn (nonlocal) potential, while the dashed line signifies the Argonne V18 potential. Results derived from the CD-Bonn potential exhibit a relatively softer trend, leading to a lower maximum neutron star mass, which falls below recent observational measurements. Conversely, outcomes derived from the Argonne V18 + TBF (local) potential demonstrate a stiffer behavior, with a maximum mass of 2.13 $M_\odot$ and a corresponding radius of 8.6 km. This maximum mass value aligns with the largest observed mass to date, (2.14 ± 0.10) $M_\odot$ [26] for PSR J0740+6620, and is consistent with other theoretical predictions [27].

The differences in the neutron star masses obtained using CD-Bonn and Argonne V18 potentials stem from the non-local nature of the CD-Bonn potential. Specifically, the CD-Bonn potential includes strong non-localities that resulting in larger $^3S_1$ wave functions at distances less than 0.8 fm, and softer repulsive cores compared to the local potential. While these differences in the potentials' predictions for many-body systems are less pronounced than those observed with older potentials. Consequently, selecting for the local representation may be more suitable in this scenario due to its simplicity, enabling more precise many-body calculations [28].

Table (1): The characteristics of the configuration with the maximum mass acquired for various potentials. $M_G/M_\odot$ represents the gravitational (maximum) mass, along with the associated radius (R) and central number density (nc).

Model	$M_G/ M_\odot$	R(km)	n_c (fm^{-3})
CD-Bonn	1.32	5.22	1.97
Argonne V18	1.50	5.56	1.98
CD-Bonn +TBF	1.71	9.1	1.39
Argonne V18 + TBF	2.12	9.2	1.35
Argonne V14 + TBF	1.8	9.7	1.34 [30]
Paris potential + TBF	1.94	9.54	1.33 [30]
PSR J0621+1002	1.70 ± 0.5		[30]
PSR J0740+6620	2.14		[26]

In table 1. A comparison of the properties associated with the maximum mass configuration for the adopted models, along with the results from [29] in case of two-body force only. As expected, the addition of nuclear TBF leads to larger masses than calculations solely considering two-body forces. This discrepancy reflects the significant modification of the maximum mass configuration and the EOS resulting from nuclear TBF. The table further compares our results with those derived from two other NN interactions: the local Argonne V14 and the non-local Paris potentials, both implemented with the same TBF from [30]. Notably, there are significant variations in maximum masses across these scenarios, confirming the sensitivity of results to the specific choice of NN interaction and TBF.

IV. CONCLUSIONS

The microscopic equation of state (EOS) incorporated by the Three-Body Forces (TBF) has been computed at extremely high densities for pure neutron matter at absolute zero temperature, employing the Brueckner-Hartree-Fock (BHF) method with the CD-Bonn and Argonne V18 nucleon-nucleon (NN) potentials. The addition of the TBF within the Urbana model has been used in order to improve the saturation properties.

In our calculations, the analysis reveals a proximity of both saturation characteristics to the empirical value .

Notably, the calculation of BHF with the inclusion of TBF illustrate a stiffer EOS with the Argonne V18 NN potential compared to the CD-Bonn variant. Within the microscopic EOS, neutron star mass-radius relationships have been established using the Tolman-Oppenheimer-Volkoff (TOV) equation with compatible way. The adopted Argonne V18 potential, our calculations align with observed neutron star masses [26] (PSR J0740+6620), while despite the softer nature of the maximum mass calculated with the CD-Bonn potential compared to Argonne V18, it concurs with measured neutron star masses, notably those observed by Splaver (PSR J0621+1002) [31, 32]. However, the limiting masses, radii, and central densities generated by both interactions are relatively close to each other. It is emphasized that the inclusion of TBF is crucial in deriving the microscopic EOS and neutron star parameters. Additionally, configurations such as maximum masses and radii of neutron stars are sensitive by modern NN potentials.

ACKNOWLEDGMENTS

The author expresses gratitude for the helpful discussions with Professors Khalaf Gad and Khaled Hassaneen. Additionally, acknowledgment is extended to Professor Morten Hjorth-Jensen for offering code possibilities.

REFERENCES

[1] M. Baldo (Ed.), Nuclear, Methods and the Nuclear Equation of State, International Review of Nuclear Physics, vol. 8, World Scientific, 1999 (Chapter 1).

[2] J. P. Jeukenne, A. Lejeune, and C. Mahaux, Physics Reports 25, 83 (1976).

[3] R. Brockmann and R. Machleidt, Physical Review C 42, 1965 (1990); G. Q. Li, R. Machleidt, and R. Brockmann, Physical Review C 45, 2782 (1992); P. G. Krastev and F. Sammarruca, Physical Review C 74, 025808 (2006).

[4] D. Alonso and F. Sammarruca, Physical Review C 67, 054301 (2003).

[5] J. Carlson, V. R. Pandharipande, and R. B. Wiringa, Nuclear Physics A 401, 59 (1983).

[6] A. Akmal, V. R. Pandharipande, and D. G. Ravenhall, Physical Review C 58, 1804 (1998); J. Morales, V. R. Pandharipande, and D. G. Ravenhall, Physical Review C 66, 054308 (2002).

[7] B. S. Pudliner, V. R. Pandharipande, J. Carlson, and R. B. Wiringa, Physical Review Letters 74, 4396 (1995); Physical Review C 56, 1720 (1997).

[8] J. Carlson and R. Schiavilla, Reviews of Modern Physics 70, 743 (1998); R. B. Wiringa, S. C. Pieper, J. Carlson, and V. R. Pandharipande, Physical Review C 62, 014001 (2000); S. C. Pieper, K. Varga, and R. B. Wiringa, Physical Review C 66, 044310 (2002); M. Pervin, S. C. Pieper, and R. B. Wiringa, Physical Review C 76, 064319 (2007).

[9] X. R. Zhou, F.G. Burgio, U. Lombardo, H.-J. Schulze, W. Zuo, Physical Review C 69 (2004) 018801.

[10] H. Heiselberg and M. Hjorth-Jensen, Physics Reports 328/5-6, 237-327 (2000).

[11] M. Baldo and Alaa Eldeen Shaban, Physics Letters B 661, 373 (2008).

[12] J. M. Lattimer and M. Prakash, The Astrophysical Journal 550, 426 (2001).

[13] J. M. Lattimer and M. Prakash, Physics Reports 442, 109 (2007).

[14] Bethe H.A., *Annual Review* of *Nuclear and Particle Science* 21, 93 (1971).

[15] M. Baldo, G. Giansiracusa, U. Lombardo, H.Q. Song, Physics Letters B 473 (2000) 1.

[16] M. Baldo, A. Fiasconaro, G. Giansiracusa, U. Lombardo, H.Q. Song, Physical Review C 65 (2001) 017303.

[17] F. Coester, S. Cohen, B. D. Day and C. M. Vincent Physical Review C 1 769 (1970).

[18] S. Gandolfi, A. Gezerlis and J. Carlson, *Annual Review* of *Nuclear and Particle Science* 65 303 (2015).

[19] W. Zuo, A. Lejeune, U. Lombardo, J. F. Mathiot, Nuclear Physics A 706, 418 (2002).

[20] Z.H. Li, U. Lombardo, H.J. Schulze, W. Zuo, Physical Review C 77, 034316 (2008).

[21] Wiringa R.B., Fiks V. and Fabrocini A., Physical Review C 38, 1010 (1988).

[22] M. Baldo, C. Maieron, Physical Review C 72 (2005) 034005.

[23] Burrows, A. Perspectives on Core-Collapse Supernova Theory. Reviews of Modern Physics 85, 245 (2013).

[24] Tolman, R. C., Proceedings of the National Academy of Sciences (USA), 20, 3 (1934).

[25] Oppenheimer, J., Volkoff, G., Physical Review 55, 374 (1939).

[26] Cromartie, H. T., Fonseca, E., Ransom, S. M., et. al., Nature Astronomy, 4, 72 (2020).

[27] G. F. Burgio; H.-J. Schulze; I. Vida˜na; J.-B. Wei. Symmetry 13, 400 (2021).

[28] L. Engvik, M. Hjorth-Jensen, R. Machleidt, H. M¨uther and A. Polls, Nuclear Physics A 627, 85 (1997).

[29] Abou-Elsebaa, H.M., Darwish, E.M., Hassaneen, K.S. Moscow University Physics Bulletin 75, 320–330 (2020).

[30] M. Baldo, I. Bombaci and G. F. Burgio, Astronomy and Astrophysics

328, 274 (1997).

[31] M. Eric Splaver et. al., The Astrophysical Journal 581 509 (2002).

[32] C.M. Zhang et. al., Astronomy and Astrophysics 527, id.A83, 8 pp. (2011).